Environmental Science & Technology

pubs.acs.org/est

Article

Triple Isotopes ($\delta^{13}C$, $\delta^{2}H$, and $\Delta^{14}C$) Compositions and Source Apportionment of Atmospheric Naphthalene: A Key Surrogate of Intermediate-Volatility Organic Compounds (IVOCs)

Tiangang Tang, Zhineng Cheng,* Buqing Xu, Bolong Zhang, Sanyuan Zhu, Hairong Cheng, Jun Li, Yingjun Chen, and Gan Zhang*

Cite This: *Environ. Sci. Technol.* 2020, 54, 5409−5418

Read Online

ACCESS | Metrics & More | Article Recommendations | Supporting Information

ABSTRACT: Naphthalene (NAP), as a surrogate of intermediate-volatility organic compounds (IVOCs), has been proposed to be an important precursor of secondary organic aerosol (SOA). However, the relative contribution of its emission sources is still not explicit. This study firstly conducted the source apportionment of atmospheric NAP using a triple-isotope ($\delta^{13}C$, $\delta^{2}H$, and $\Delta^{14}C$) technique combined with a Bayesian model in the Beijing−Tianjin−Hebei (BTH) region of China. At the urban sites, stable carbon (−27.7 ± 0.7‰, $\delta^{13}C$) and radiocarbon (−944.0 ± 20.4‰, $\Delta^{14}C$) isotope compositions of NAP did not exhibit significant seasonal variation, but the deuterium system showed a relatively more ^{2}H depleted signature in winter (−86.7 ± 8.9‰, $\delta^{2}H$) in comparison to that in summer (−56.4 ± 3.9‰, $\delta^{2}H$). Radiocarbon signatures indicated that 95.1 ± 1.8% of NAP was emitted from fossil sources in these cities. The Bayesian model results indicated that the emission source compositions in the BTH urban sites had a similar pattern. The contribution of liquid fossil combustion was highest (46.7 ± 2.6%), followed by coal high-temperature combustion (26.8 ± 7.1%), coal low-temperature combustion (18.9 ± 6.4%), and biomass burning (7.6 ± 3.1%). At the suburban site, the contribution of coal low-temperature combustion could reach 70.1 ± 6.4%. The triple-isotope based approach provides a top-down constraint on the sources of atmospheric NAP and could be further applied to other IVOCs in the ambient atmosphere.

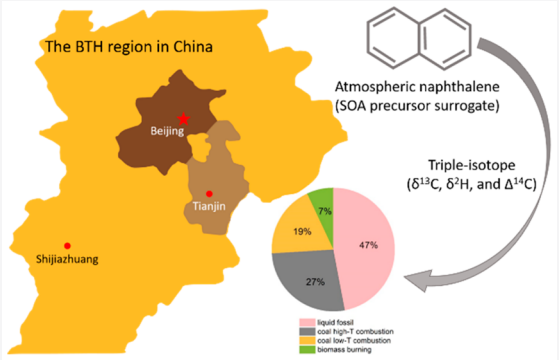

INTRODUCTION

Widely existing in the atmosphere, naphthalene (NAP) is worthy of concern not only due to its carcinogenicity but also as an important precursor of atmospheric SOA. NAP, as a fusion of two benzene rings, is the most abundant polycyclic aromatic hydrocarbon (PAH) in the ambient atmosphere. NAP shows adverse effects on human health.[1,2] The US Department of Health and Human Services and the International Agency for Research on Cancer had both reached the conclusion that NAP is reasonably listed as a human carcinogen.[3,4] However, recently, NAP was more addressed for its potentially important contribution to secondary organic aerosol (SOA).[5−9] It was recognized as a surrogate compound of intermediate-volatility organic compounds (IVOCs) in studies concerning IVOCs and SOA.[10] Chan et al.[6] reported that the SOA yields of NAP and MN (methylnaphthalene) were 25−45% and 55−75% under high- and low-NO_x conditions, respectively. Huang et al.[11] estimated that NAP and MN could contribute to the production of about 14.9% of the SOA formed in the afternoon during a wintertime haze in Beijing, which is comparable to the contribution from light aromatics (e.g., toluene and benzene) on SOA formation.

Potential emission sources of NAP include motor vehicle exhaust, coal combustion, biomass burning, metal and chemical industries, and substances containing NAP (e.g., mothballs, slow-curing asphalt).[12] However, the major sources and their corresponding contributions to atmospheric NAP remain poorly understood. Lu et al.[13] estimated NAP emission rates from major sources in southern California by bottom-up emission inventory techniques. However, this method is restricted by the uncertainties in estimating both activity volume and emission factors.[14] Top-down constraints with the intrinsic isotopic compositions of the specific compounds can help to narrow the uncertainties in source analyses. Stable carbon isotope ($\delta^{13}C$) analysis on specific compounds has been widely used to study the origins and sinks of contaminants.[15−17] Meanwhile, the stable hydrogen isotope

Received: January 5, 2020
Revised: April 6, 2020
Accepted: April 7, 2020
Published: April 7, 2020

https://dx.doi.org/10.1021/acs.est.0c00075
Environ. Sci. Technol. 2020, 54, 5409−5418

(δ^2H), in comparison with δ^{13}C, could be a more powerful tool for source apportionment because δ^2H values of some compounds emitted from different sources or produced through different conversion processes have a much greater degree of differentiation.[18−22] In addition to these stable isotopes, compound-specific radiocarbon analysis (CSRA) can distinguish sources of target compounds between fossil fuel (void of ^{14}C) and nonfossil (contemporary ^{14}C) sources unambiguously.[23,24] Bosch et al.[25] applied a triple-isotope system (δ^{13}C, Δ^{14}C, and δ^2H) to elucidate the relative contributions of four major sources of PAHs (not including Nap) in central European forest soils. As far as we know, there are still no reports about the triple-isotope composition of atmospheric two-ring PAHs.

The BTH region is China's "Capital Economic Circle" and has been subjected to intensive atmospheric pollution mitigation campaigns since 2013. During haze events, a large portion of particulate matter was identified to be SOA.[26] Considering the fact that NAP is an important precursor of SOA, a further study of NAP sources is essential to improve air quality. Therefore, the objectives of this study were (1) to investigate the spatiotemporal variation of concentration and isotopic signatures (δ^{13}C, δ^2H, and Δ^{14}C) of atmospheric NAP in the BTH region and (2) to qualify the relative contributions of the major sources to atmospheric NAP by the triple-isotope approach. To the best of our knowledge, this study represents the first trial of using δ^{13}C−δ^2H−Δ^{14}C isotopes to identify the potential sources of NAP.

MATERIALS AND METHODS

Sampling Site. A sampling campaign was conducted simultaneously at five sites (Figure S1). Four of these were located in the BTH region. These included three urban sites (Beijing, Tianjin, and Shijiazhuang) and a suburban site (Huairou). Beijing (BJ) is the capital of China. Tianjin (TJ) is an economically developed municipality. Shijiazhuang (SJZ) is the capital of Hebei province and is a highly industrialized city. Huairou (HR) is a suburban county of Beijing, located in the northeastern region of the city. Guangzhou (GZ) was selected as a control site, which is a metropolis in southern China.

Sampling Method. High-volume samplers (Tisch, TE-1000) were used to collect gaseous-phase NAP at each site. The sampling flow was set as 200 L/min. A 20 g polystyrene−divinylbenzene resin (XAD-2) was filled into a sampling cartridge as the adsorbent for capturing gaseous-phase NAP.[27−29] Methylnaphthalene (MN) could also be collected at the same time. The sampling time was from February 25 to March 6 (winter), April 5 to 15 (spring), and July 5 to 15 (summer) in 2018.

To detect any possible breakthrough, the XAD-2 resin was divided into two independent parts by a filter screen in the cartridge: front (20 g) and backup (10 g) (Figure S2). The resin was stored in brown screw-cap jars at −20 °C before and after sampling. All high-volume samplers were set on rooftops, about 20−30 m above the ground. There were no major emission sources or highways near the sampling sites. Quartz fiber filters (QFF) and XAD-2 resin were replaced on a daily schedule to limit the potential breakthrough. Details about the sampling method are presented in the Supporting Information.

Quantification of NAP and MN. Partial XAD-2 resin samples were taken out to quantify the concentration of NAP and MN. The XAD-2 resin samples were spiked with deuterated NAP ($C_{10}D_8$) before extraction to assess analytical process losses and then extracted by Soxhlet extraction with dichloromethane (DCM) for 24 h. The extract was concentrated and filtered. Hexamethylbenzene was added as an internal standard. NAP and MN were analyzed by a gas chromatograph−mass spectrometer (GC-MS) system (Agilent 7890A GC coupled with a 5975B MS) in selective ion monitoring (SIM) mode. Gas chromatographic separations were performed on a 30 m DB-5 ms capillary column (0.25 mm i.d.; 0.25 μm df; J&W).

Analytical procedures were performed strictly to ensure quality control. One experimental blank was conducted every 10 samples. The method detection limits of NAP (MDL) was averaged at 0.006 ± 0.003 μg/m^3 (n = 5). A NAP measurement was acceptable only when its recovery rate was in the range of 60−75%. Field blanks of XAD-2 resin were taken to represent potential contamination of sample transportation and experimental treatment. The concentrations of NAP and MN in the field blank samples were 1−5% of the detected concentrations in atmospheric samples, indicating limited background contamination. After 24 h of sampling, the breakthrough rate (the ratio of captured NAP found in the front/backup part) was less than 10%, which was within the acceptable breakthrough criteria for quantitative sampling.[30] Further details of the quantitative process are included in the Supporting Information.

Extraction of NAP and MN for Isotope Analyses. The XAD-2 resin samples used for isotope analyses were not spiked with deuterated NAP before extraction. Extracts were concentrated, and solvent was exchanged into hexane by rotary evaporation after Soxhlet extraction. Subsequently, the extracts were precleaned by a chromatography column of silica gel and alumina. After precleaning, NAP and MN could be baseline separated from other interfering compounds by gas chromatography (Figure S3). The treated samples were concentrated to the appropriate concentration by gentle nitrogen blowing for stable carbon and hydrogen isotope analyses, respectively. Further details about the purification are presented in the Supporting Information.

Analysis of Stable Carbon and Hydrogen Isotopes. The stable carbon and hydrogen isotope compositions of NAP and MN were acquired by a gas chromatograph−isotope ratio mass spectrometer system (GC-IRMS). The system consisted of a Trace 1310 GC instrument (Thermo Fisher Scientific) equipped with a 30 m capillary column (Agilent, DB-5MS; 0.25 mm i.d., 0.25 mm film thickness) and a Delta V Advantage isotope ratio mass spectrometer (Thermo Fisher Scientific). The GC and IRMS were connected by a GC Isolink and Conflo IV interface (Thermo Fisher Scientific).

To monitor the precision and accuracy of measurements, a standard mixture of n-alkanes (C12, C14, C16, C18, C20, C22), purchased from Indiana University, with a known isotopic composition was analyzed daily for both δ^{13}C and δ^2H. On comparison of the measured values with the known values of these standard samples, standard deviations should be better than 0.5‰ for δ^{13}C and 5‰ for δ^2H, respectively. The H_3^+ factor was determined daily prior to hydrogen isotope analyses (the H_3^+ value was stable at 6.12−6.23 ppm/nA during the analysis). The reported isotope results were the arithmetic means of triplicate analyses. The δ^{13}C and δ^2H values are reported as the (per mil, ‰) deviation of the isotope value of Peedee belemnite (VPDB) and Vienna Standard Mean Ocean Water (VSMOW), respectively. Experimental treatment would not affect the original isotopic

https://dx.doi.org/10.1021/acs.est.0c00075
Environ. Sci. Technol. 2020, 54, 5409−5418

signatures (Table S2).[31] The differences in $\delta^{13}C$ values of NAP extracted from the front and backup resins were within the accuracy of the instrument (<0.5‰). Further information on the instrumental analyses is provided in the Supporting Information.

Individual Compound Isolation and Radiocarbon Analyses. Preparative capillary gas chromatography (PCGC) was used to isolate NAP and MN. To provide sufficient NAP and MN for radiocarbon analyses, extracts of several days of samples from the same site and the same season were combined after precleaning. The concentrated extracts were injected repeatedly into the PCGC system. The PCGC system consisted of a gas chromatograph (7890A, Agilent) with an FID detector coupled to a cooled injection system (CIS 3, Gerstel) and a preparative fraction collector (PFC, Gerstel). 1-Methylnaphthalene (1-MN) and 2-methylnaphthalene (2-MN) were trapped in the same tube because of their relatively low contents. The injections were fixed to 60 times for each sample. The recovery rate of the isolation procedure could be stabilized at over 80%. After preparation, the isolated NAP and MN were graphited (AGE 3, Ionplus) and analyzed for ^{14}C by accelerator mass spectrometry (AMS) (NEC 0.5MV 1.5SDH-2, National Electrostatics Corporation, USA) at the Guangzhou Institute of Geochemistry, Chinese Academy of Sciences. To evaluate the amount of introduced extraneous carbon, the fraction modern (Fm) values of standard NAP (with dead ^{14}C composition) and *n*-docosane (with modern ^{14}C composition) were determined before and after treatment (chemical treatment and monomer isolation). The introduced extraneous carbon would cause a deviation in the consensus Fm values. The modern carbon contamination was calculated with the isotopic offsets from the original Fm values of NAP, whereas the isotopic offsets from the original Fm values of *n*-docosane would gave the dead carbon contamination.[32] The Fm values of samples were expressed by the equation

$$Fm_{sample} \times C_{sample} = Fm_{measured} \times C_{measured} - Fm_{ex} \times C_{ex} \quad (1)$$

where Fm_{sample} is the original radiocarbon value of standard NAP or *n*-docosane samples, $Fm_{measured}$ denotes the radiocarbon values of standard NAP or *n*-docosane samples which had been processed by chemical treatment and monomer isolation, Fm_{ex} values of extraneous dead carbon and extraneous modern carbon are 0 and 1, and C_{sample} is equivalent to $C_{measured} - C_{ex}$. The calculated amounts of introduced extraneous dead carbon and modern carbon were less than 1 and 4 μg, respectively (Figure S4). To diminish the influence of the extraneous carbon, the carbon content was above 100 μg for each sample for AMS analyses. The details can be found in the Supporting Information.

Bayesian Mixing Model for Source Apportionment. The "MixSIAR" model, the latest Bayesian isotope mixing model in R (https://cran.r-project.org/web/packages/MixSIAR/index.html), was used to qualify the contributions and uncertainties of different NAP emission sources. Further information about the model can be found in previous studies.[33,34] The input data of the MixSIAR model were the observed triple-isotope values ($\delta^{13}C$, $\delta^{2}H$, and $\Delta^{14}C$) of atmospheric NAP from the three seasons at the different sites with standard error. The fractionation values of the three isotopes were set to zero for the atmospheric transportation and chemical treatment procedures.[25,35] All effects (parameters) are considered random within the Bayesian framework. The Markov chain Monte Carlo parameter was set to "long" run length. The error options of "residual error" were specified in the model. Diagnostic tests (Gelman–Rubin, Geweke, and Heidelberger–Welch) were used to identify whether the model converged. The estimated mean proportion of each source was analyzed for comparison. The source-specific isotope values used in the simulation model are given in Table 1.

Table 1. Isotopic Signatures (End Members) for the Primary PAH Sources

primary source	isotope (mean ± std dev, ‰)		
	$\delta^{13}C$	$\delta^{2}H$	$\Delta^{14}C$
biomass burning	−26.7 ± 2.0	−96.0 ± 10.0	−137.5 ± 21.9
liquid fossil combustion	−27.4 ± 0.8	−67.5 ± 7.6	−1000 ± 0.0
coal high-*T* combustion	−27.5 ± 0.5	−61.3 ± 5.0	−1000 ± 0.0
coal low-*T* combustion	−24.1 ± 1.2	−100.0 ± 15.5	−1000 ± 0.0

RESULTS AND DISCUSSION

Ambient Concentrations and Seasonal Trends. Mean concentrations of atmospheric gaseous-phase NAP and MN at the five sampling sites are shown in Table S3. The seasonal average concentrations of NAP ranged from 0.07 to 1.16 μg/m^3, with great differences among different locations and seasons. The concentration range was similar to that reported previously in southern California (0.02–1.58 μg/m^3).[13,36,37] The mean concentration of the urban sites in the BTH region (0.73 ± 0.31 μg/m^3, $\mu \pm \sigma$) was significantly higher than that of HR (0.25 ± 0.07 μg/m^3) ($p < 0.05$). The higher NAP concentration in these northern urban sites than in the suburban site might be caused by more emission sources in the urban area, such as heavier traffic,[38] more cooking activities,[39,40] more coal used for heating (residual coal had been completely replaced by natural gas in HR in 2018),[41] and so on. Meanwhile, dense high-rise buildings in the cities could further lead to the enrichment of pollutants.[20]

As shown in Figure 1, the NAP concentrations at both the urban and suburban sites in the BTH region were in the order of winter ≈ summer > spring. The difference between winter and summer was not significant (*t* test, $p > 0.05$). However, gaseous PAH (NAP accounts for the largest portion of gaseous PAHs in typical ambient air)[11,37] concentration has been

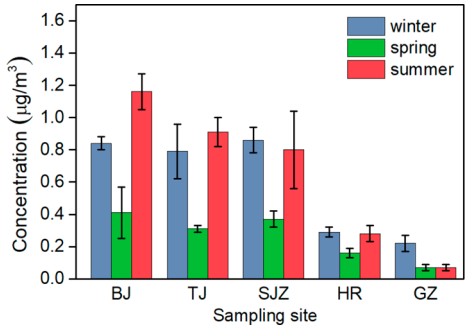

Figure 1. Mean concentration of NAP in winter, spring, and summer. Abbreviations: Beijing (BJ), Tianjin (TJ), Shijiazhuang (SJZ), Huairou (HR), and Guangzhou (GZ).

https://dx.doi.org/10.1021/acs.est.0c00075
Environ. Sci. Technol. 2020, 54, 5409–5418

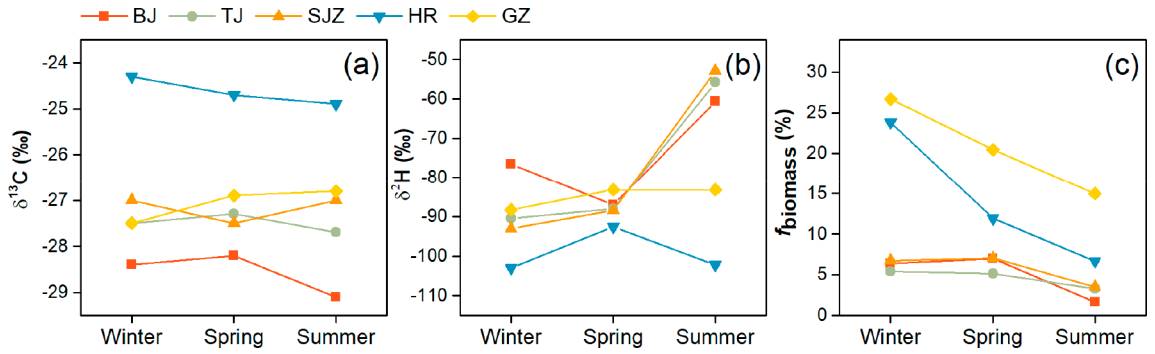

Figure 2. Temporal−spatial distribution of stable carbon (a) and hydrogen (b) isotope compositions and fraction modern (c) of atmospheric vapor-phase naphthalene. Abbreviations: Beijing (BJ), Tianjin (TJ), Shijiazhuang (SJZ), Huairou (HR), and Guangzhou (GZ).

reported to be higher in winter than in summer in Northern Chinese Plain, possibly due to the combustion of fossil fuels for heating in winter.[42,43] This inconsistent seasonal variation found in this study and former report might be attributable to the fact that residential coal, adopted as a major heating fuel in rural and suburban areas, had been widely forbidden around the sampling sites.[44] Although this unregulated residential coal accounted for only about 10% of the total coal consumption in the BTH region, it could contribute approximately half of the PAH emission due to its relatively low combustion efficiency and poor fuel quality.[44−46] Meanwhile, some industries, such as steel and chemical industries, have been forced to reduce operating rates by 30−50%, and some industries producing construction materials, such as cement, pottery, and plaster tablets, had been required to suspend production in heating periods.[47] These measures would have reduced the NAP emissions due to heating activity and industrial production in winter. Some other factors might also affect the NAP concentration. For example, lower atmospheric mixing height and slower photochemistry reaction rate in winter could accumulate more NAP concentration in the atmosphere,[42] whereas higher temperatures in summer could accelerate the volatilization of NAP-containing substances,[48] such as lubricants and bitumen. All of these factors resulted in similar NAP concentrations in winter and summer. The lower NAP concentration level in the spring is perhaps for two reasons. First, the atmospheric diffusion conditions are relatively better than those in winter. The average value of air quality index (AQI) in the spring sampling period was much lower than that in winter in these northern sites (Table S1). Second, there is relatively less industrial emission in spring than in summer. We assumed many industries had not yet resumed normal production in spring on the basis of the conclusion from the last section, that the relative contributions of the main NAP emission sources were rather homogeneous in winter and spring.

Interestingly, we found the control site GZ, in comparison with the urban sites in the BTH region, has a lower NAP concentration level (0.12 ± 0.09 $\mu g/m^3$) and a different seasonal trend (winter > spring ≈ summer). GZ is a metropolis in southern China with high population density and advanced industry. Located at the junction of the tropics and the subtropics, GZ has no heating season. In addition, there was no specific air pollution reduction program around GZ during the sampling periods. Therefore, the seasonal fluctuation in energy consumption in GZ was less than that in the northern cities. Combining the above facts, we speculated that the lower concentration and different seasonal variation tread of NAP in GZ were mainly caused by atmospheric diffusion. As a coastal city, GZ has better atmospheric diffusion conditions. Relatively clean air masses originating from marine areas would be beneficial to reducing the concentration of pollutants.[49] According to 72 h back trajectories, we found the proportions of air masses originating from the ocean during the sampling period in winter, spring, and summer were about 39%, 60%, and 100%, respectively (Figure S6).

NAP, 1-MN, and 2-MN usually coexist in some sources, such as cigarette smoke, wood smoke, tar, oil, and asphalt.[3] In this study, the concentrations of 1-MN and 2-MN had seasonal and spatial trends similar to those of NAP. The concentrations all showed a good correlation between each of the two variables of NAP, 1-MN, and 2-MN ($R^2 = 0.67$, $p < 0.01$ for NAP and 1-MN; $R^2 = 0.71$, $p < 0.01$ for NAP and 2-MN; $R^2 = 0.94$, $p < 0.01$ for 1-MN and 2-MN; Figure S7). These results verified that these compounds might have relatively similar emission sources.

Stable Carbon and Hydrogen Isotope Compositions. In this study, the $\delta^{13}C$ values of NAP ranged from −29.1‰ to −24.3‰ (Table S4). No substantial variation was found among the three seasons (one-way ANOVA, $p > 0.05$; Figure 2a). However, there were obvious spatial variations, with BJ having the lowest $\delta^{13}C$ values (-28.6 ± 0.5‰, $\mu \pm \sigma$) and HR having the highest $\delta^{13}C$ values (-24.6 ± 0.3‰). The other three urban sites (TJ, SJZ, and GZ) had similar $\delta^{13}C$ values (-27.2 ± 0.3‰). Although there are limited literature reports about the $\delta^{13}C$ values of atmospheric NAP, several studies reported the $\delta^{13}C$ values of PAHs derived from aerosols.[50,51] As a PAH, the $\delta^{13}C$ values of NAP can be compared to those of 3−4-ring PAHs. The reported $\delta^{13}C$ values of 3−4-ring atmospheric PAHs in some large cites in China range from −26.5‰ to −24.4‰[16,52] (3-ring PAHs, − 25.4‰ to −25.0‰ in Zhengzhou and −26.5‰ to −24.7 ‰ in Urumchi; 4-ring PAHs, −24.8‰ to −24.4‰ in Chongqing and Hangzhou and −25.5‰ to −24.8‰ in Beijing). The $\delta^{13}C$ values of NAP at the urban sites in this study were much more ^{13}C depleted than these 3−4-ring PAHs in former reports. It is generally acknowledged for automotive exhausts that the isotopic trend of PAHs becomes more ^{13}C enriched with increasing molecular weight.[50] However, for coal combustion emission, the trend is opposite.[53] The relatively more depleted $\delta^{13}C$ values of NAP might indicate that a larger proportion of the NAP in this study was emitted from motor vehicle exhaust. Another possible reason is that the use of residential coal had already been banned in the study areas.[44] PAHs released from residential coal have heavier isotopic values in comparison to those from industrial coal. Peng et al.[52] reported that the mean

https://dx.doi.org/10.1021/acs.est.0c00075
Environ. Sci. Technol. 2020, 54, 5409−5418

$\delta^{13}C$ values of phenanthrene in soot from residential coal and industrial coal combustion were −22.0‰ and −23.1‰, respectively. Residential coal-derived PAHs are released as primary devolatilization products with little structural change. Their isotopic signatures are basically similar to those of the parental coal.[54] However, in industrial coal use, such as high-temperature combustion and gasification, the conversion processes are more intensive. The majority of industrial coal-derived PAHs results from ring growth, involving carbon−carbon bond formation, cyclization, and ring fusion, which results in a kinetic isotope effect in which $^{12}C-^{12}C$ bonds form more easily than $^{13}C-^{12}C$ bonds.[25] Therefore, PAHs emitted from industrial coal have relatively light isotopic values.

Studies of the δ^2H values of atmospheric organic compounds remain limited. As far as we know, this is the first report of the δ^2H values of atmospheric NAP. The δ^2H values of NAP ranged from −103.0‰ to −52.8‰ (−83.4 ± 14.3‰). The δ^2H values were much more enriched in comparison to those of 3-ring PAHs in forest soils from the Czech Republic[25] (−114.7 ± 40.7‰). In contrast to the stable carbon isotope, the deuterium isotope showed higher variability among both sites and seasons (Figure 2b). It is interesting that the δ^2H values of NAP were obviously much heavier in summer than in winter and spring at all of the urban sites in the BTH region, whereas the δ^2H values of NAP in winter and summer were roughly equal in GZ. This might has been caused by shutdowns or cutbacks in many industries during the heating period in the BTH region,[47] and these industries had not fully resumed production during the spring sampling period. These results suggest that NAP from these industrial sources has a relatively heavy δ^2H value.

A negative correlation was found between the $\delta^{13}C$ and δ^2H values of NAP ($R^2 = 0.33$, $p < 0.05$), which is consistent with the study by Sun.[19] For PAHs, enrichment in ^2H occurs simultaneously with ^{13}C depletion in the polyaromatization process because the lighter hydrogen isotopes are preferentially removed from the newly formed PAH ring structures and $^{12}C-^{12}C$ bonds form more easily than $^{13}C-^{12}C$ bonds. The isotopic compositions of 1-MN and 2-MN shared a similar seasonal and spatial trend with NAP. Both the $\delta^{13}C$ and δ^2H values of NAP had a significant correlation with those of MN (Figures S8 and S9).

Radiocarbon Isotope Composition. Unlike the uncertainty present in the source apportionment with stable carbon and hydrogen isotopes, radiocarbon (^{14}C) measurements allow unambiguous distinction of sources between fossil fuels and biomass. The relative contributions of fossil and biomass sources to atmospheric NAP can be estimated from the equation

$$\Delta(^{14}C_{NAP}) = \Delta(^{14}C_{biomass})f_{biomass} + \Delta(^{14}C_{fossil})(1 - f_{biomass}) \quad (2)$$

where $\Delta^{14}C_{NAP}$ is the measured radiocarbon content of NAP and $f_{biomass}$ and $(1 - f_{biomass})$ are the fractions of NAP derived from biomass and fossil sources, respectively. $\Delta^{14}C_{fossil}$ is −1000‰ because all ^{14}C is completely depleted, and $\Delta^{14}C_{biomass}$ was +137.5‰, which was calculated assuming equal proportions of wood (+225‰) and fresh biomass (+50‰).[25] The measured $\Delta^{14}C$ values of NAP ranged from −973.6‰ to −696.3‰ (Table S5). The corresponding $f_{biomass}$ ranged from 0.02 to 0.27, indicating that fossil fuels were the major sources of atmospheric NAP at these sampling sites. There was notable seasonal and spatial variation, as shown in Figure 2c. The $f_{biomass}$ values of NAP in winter and spring samples were significantly higher than those in summer samples for all sampling sites (t test, $p < 0.01$). Airborne PAHs with modern carbon are almost all released from biomass or biofuel burning.[55−57] Because the use of biofuels remains very limited in China,[58] we assumed that the majority of NAP with modern carbon was released from biomass burning. This inference is consistent with the results showed in fire count maps, in which more wildfires surrounding the sampling sites occurred in winter and spring than in summer (satellite-based moderate resolution imaging spectroradiometer (MODIS); Figure S5). Meanwhile, fire counts were roughly equal between winter and spring at urban sites in the BTH region, which corresponds with the $f_{biomass}$ values of NAP. However, for HR, the $f_{biomass}$ values of NAP were obviously greater in winter (0.24) than in spring (0.12). This might indicate that residential biomass burning for winter heating still was happening in rural or suburban areas in the BTH region during the sampling period. The $f_{biomass}$ values of NAP in GZ (0.27 and 0.15) were obviously larger than those in the BTH urban region and were even slightly larger than those at the suburban site (HR). This might have occurred because southern China is more affected by biomass burning or has some specific biological sources. A series of studies have indicated PAHs, especially low-molecular-weight PAHs, had several specific biological origins in tropical zones, such as some tropical plants, fungi, and bacteria in termite mounds.[59,60] GZ is located at the junction of the tropics and the subtropics. However, relevant research about the specific biological sources of PAHs is still scarce in the area of GZ. In addition, the coal consumption in Guangdong province was also much lower than that in Hebei province. According to data from the National Bureau of Statistics of China, the coal consumptions in 2016 in Guangdong and Hebei were 16135 and 28105 million tons, respectively.

The fraction of NAP ($f_{biomass}$) derived from biomass in this study was similar to that of PAHs reported by other researchers. The $f_{biomass}$ values for PAHs derived from the aerosol in North Birmingham,[61] Greece,[56] and Croatia,[56] which were also obtained by compound-specific radiocarbon analysis (CSRA), were 4%, 7%, and 9% respectively. In addition, some studies estimated the $f_{biomass}$ values of atmospheric aromatic compounds in cities in China by molecular marker and statistical analyses. Yuan et al.[62] predicted biomass burning contributions of 9.5% for benzene and 9.7% for toluene in the Pearl River Delta through the source-tracer-ratio (STR) method. Mao et al.[49] estimated the biomass burning contribution to the particulate PAHs was 11−14% in Ningbo, an eastern coastal city in China, by positive matrix factorization (PMF).

Source Apportionment by Bayesian Mixing Model. The compound-specific triple-isotope approach allows elucidation of the relative contributions of four emission sources to NAP. However, we did not find an emission inventory made specifically for NAP in China. Considering that NAP is a PAH, we assumed that it is also emitted mainly as a byproduct of incomplete combustion.[63] On the basis of existing bottom-up PAH emission inventories in China,[64] the primary sources are roughly categorized into biomass, coal, and liquid fossil fuels. The use of stable carbon isotopes is already a well-established technique for source apportionment.[15,25] Combustion-generated NAPs derived from C3 plants (−26.7 ± 2.0‰) and C4

https://dx.doi.org/10.1021/acs.est.0c00075
Environ. Sci. Technol. 2020, 54, 5409−5418

plants (−16.4 ± 0.8‰) are isotopically distinct.[15] The $\delta(^{13}C)$ values of NAP in samples (−27.1 ± 1.3‰) were quite different from the endmember ranges for C4 plant burning. Therefore, we inferred that the contribution of C4 plant burning to NAP in the sampling areas was minimal, and we defined the isotopic endmembers of biomass burning using the values of C3 plants. Because the $\delta(^{13}C)$ values of PAHs derived from coal combustion have a wide range (−29.4‰ to −23.0‰),[19,53,65,66] which overlaps with those for the combustion of C3 plants (−28.8‰ to −26.3‰)[15] and liquid fossil fuels (−28.1‰ to −26.5‰),[18,50] we separated the coal combustion source into two categories: high- and low-temperature combustion. This category scheme was also applied in Bosch's research.[25] Coal high-temperature (high-*T*) combustion is an intense conversion process, which is mainly applied in industry. Coal low-temperature (low-*T*) combustion is a relatively mild conversion process, generally referred to residential coal combustion. Finally, four sources, i.e., combustion of biomass, liquid fossil fuels, and coal combustion at low and high temperature, were chosen to perform the source apportionment with the Bayesian model. Because of very few scientific research reports of the source-specific $\delta^{13}C$ and $\delta^{2}H$ values of NAP, we referred to the corresponding values of phenanthrene or bulk matrix for endmember value determination of primary NAP sources. Source-specific $\delta(^{13}C)$ and $\delta(^{2}H)$ values reported in related literature are compiled in Table S6. The averages and standard deviations of isotope values from different sources were calculated. To reduce the overlapping area of high-*T* coal combustion and liquid fossil sources, we narrowed down the uncertainty range of hydrogen isotope endmember of high-*T* coal combustion source to 5‰. Table 1 gives the final endmember isotopic signatures ($\delta^{13}C$, $\delta^{2}H$, and $\Delta^{14}C$) determined in the model simulation. Figure 3 shows the 2D dual-isotope signature distribution relationship between sample data and primary sources.

The simulation results of the Bayesian model based on the triple-isotope composition are shown in Figure 4 and Figure S10. Biomass burning was the least important source of NAP in all samples, with contributions ranging between 3.5% and 21.1% (9.3 ± 4.8%). The urban site samples (BTH and GZ) showed a similar source pattern, with the highest contribution coming from the liquid fossil fuel combustion source, from 36.8% to 51.3% (45.0 ± 4.1%). Meanwhile, the contributions of coal low-*T* and high-*T* combustion sources (25.4 ± 5.2% and 19.8 ± 6.3%, respectively) were practically equal. However, for the suburban site, the major source was coal low-*T* combustion, which accounted for 70.1 ± 5.3% of the total. The relative contributions of the four different sources were rather homogeneous in winter and spring. When these two seasons were compared with summer, the contributions of coal combustion showed an obvious alternation. For the BTH urban sites, the relative contributions of the coal low-*T* combustion source changed from 22.6% to 11.5%, while that of the coal high-*T* combustion source increased from 22.8% to 34.9%, respectively.

Because the government of China had invested a large amount of effort to implement the coal substitution policy ("coal to gas" or "coal to electricity") in the BTH region, which aims to drastically reduce the use of scattered coal, no scattered coal use practices were found around the sampling sites during the sampling periods. However, according to the results of the Bayesian mixing model, the mean coal low-*T* combustion

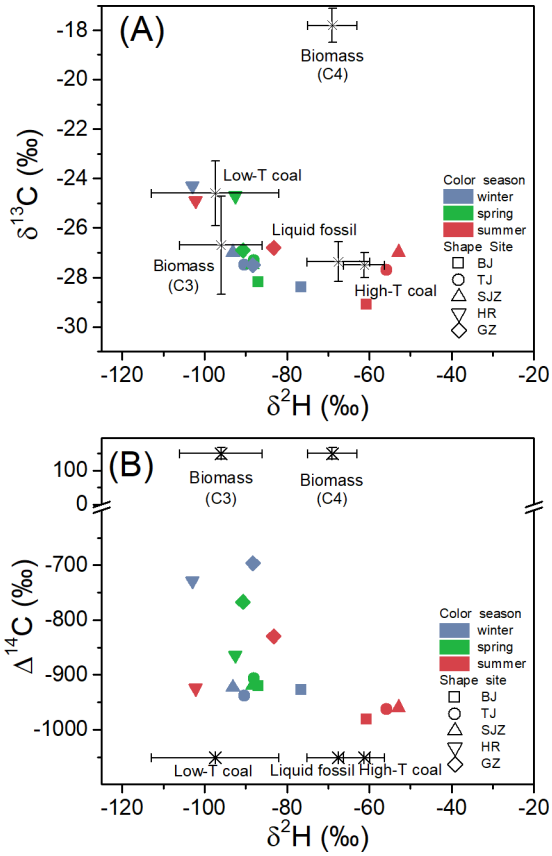

Figure 3. 2D dual-isotope signatures of samples (point symbols) and primary sources (cross range), where symbol shapes and colors are based on sampling sites and seasons, respectively: (A) $\delta^{2}H$ versus $\delta^{13}C$; (B) $\delta^{2}H$ versus $\Delta^{14}C$. Abbreviations: Beijing (BJ), Huairou (HR), Tianjin (TJ), Shijiazhuang (SJZ), and Guangzhou (GZ).

source contributions in BJ and HR were about 20% and 70%, respectively, which means that this portion of the NAP was introduced by atmospheric transport from surrounding rural areas where scattered coal was still used. BJ and HR are geographically proximal. As a result of atmospheric mixing, the NAP concentrations contributed by the coal low-*T* combustion source in BJ and HR should be comparable. This inference is consistent with the calculation results by the mean probability estimation of the coal low-*T* combustion source contribution and the field observation concentration of NAP between BJ and HR (Table 2).

This case study provides evidence that the Bayesian approach can be applied to source apportionment of atmospheric NAP. However, the accuracy of the calculation results might be affected by three factors. The first is emission sources. Four major sources were chosen to perform the Bayesian calculation model simulation in this study. However, these sources were determined on the basis of the emission inventory of PAHs in China. In comparison to other PAHs, NAP might have some specific emission sources, such as moth repellents and slow-cure asphalt.[12,13] This would have an effect on the source selection for model simulation. The second is endmembers and uncertainties. Because of the limited research, source-specific isotope signatures of NAP were partially substituted with those of phenanthrene or bulk material in this study. To improve the accuracy of the model simulation results, more source specific isotopic character-

https://dx.doi.org/10.1021/acs.est.0c00075
Environ. Sci. Technol. 2020, 54, 5409−5418

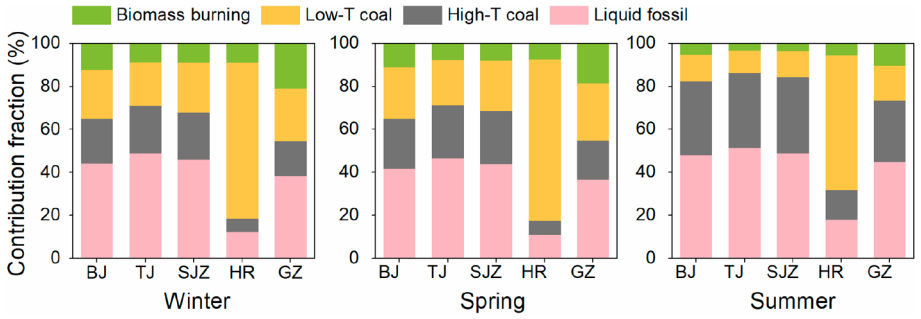

Figure 4. Source contribution of biomass burning, coal low-*T* combustion, coal high-*T* combustion, and liquid fossil combustion for vapor-phase naphthalene. Abbreviations: Beijing (BJ), Huairou (HR), Tianjin (TJ), Shijiazhuang (SJZ) and Guangzhou (GZ).

Table 2. Comparison of Naphthalene Concentration Contributed from Coal Low-*T* Combustion Sources between BJ and HR

	C_{field},[a] n = 4, $\mu g\ m^{-3}$		$f_{coal\ low\text{-}T\ combustion}$[b]		$C_{coal\ low\text{-}T\ combustion}$,[c] $\mu g\ m^{-3}$	
season	BJ	HR	BJ	HR	BJ	HR
winter	0.84 ± 0.04[d]	0.29 ± 0.03	0.23 ± 0.14	0.72 ± 0.16	0.19 ± 0.12	0.21 ± 0.05
spring	0.41 ± 0.16	0.16 ± 0.03	0.24 ± 0.12	0.75 ± 0.15	0.10 ± 0.06	0.12 ± 0.03
summer	1.16 ± 0.11	0.28 ± 0.05	0.12 ± 0.08	0.63 ± 0.18	0.14 ± 0.10	0.18 ± 0.06

[a] C_{field} denotes naphthalene concentration in field observation. [b] $f_{coal\ low\text{-}T\ combustion}$ denotes mean probability estimate from coal low-*T* combustion. [c] $C_{coal\ low\text{-}T\ combustion}$ denotes naphthalene concentration contributed from coal low-*T* combustion source; $C_{coal\ low\text{-}T\ combustion} = C_{field} f_{coal\ low\text{-}T\ combustion}$. [d] Mathematical mean ± standard deviation;

ization should be performed. The third is isotope fractionation. The fractionation factors for both stable carbon and hydrogen isotopes were set to zero in the Bayesian calculations. Changes in the $\delta^{13}C$ value of NAP in the processes of evaporation, photodecomposition, and microbial degradation are insignificant.[25,35] We assumed that hydrogen isotope fractionation is also insignificant because deuterium fractionation is generally accompanied by a change in $\delta^{13}C$ value.[25,67] Nevertheless, hydrogen isotope fractionation of NAP has not been studied systematically in environmental processes.

■ ASSOCIATED CONTENT

Supporting Information

The Supporting Information is available free of charge at https://pubs.acs.org/doi/10.1021/acs.est.0c00075.

Details about sampling and experimental treatment processes, concentrations and triple-isotope compositions of sampled NAP, 1-MN, and 2-MN, and parameters and results of the Bayesian model simulation (PDF)

■ AUTHOR INFORMATION

Corresponding Authors

Zhineng Cheng − *State Key Laboratory of Organic Geochemistry and Guangdong Key Laboratory of Environmental Protection and Resources Utilization, Guangzhou Institute of Geochemistry, Chinese Academy of Sciences, Guangzhou 510640, People's Republic of China;* orcid.org/0000-0002-6598-849X; Phone: +86-20-83853408; Email: chengzhineng@gig.ac.cn

Gan Zhang − *State Key Laboratory of Organic Geochemistry and Guangdong Key Laboratory of Environmental Protection and Resources Utilization, Guangzhou Institute of Geochemistry, Chinese Academy of Sciences, Guangzhou 510640, People's Republic of China;* orcid.org/0000-0002-9010-8140; Phone: +86-20-85290805; Email: zhanggan@gig.ac.cn

Authors

Tiangang Tang − *State Key Laboratory of Organic Geochemistry and Guangdong Key Laboratory of Environmental Protection and Resources Utilization, Guangzhou Institute of Geochemistry, Chinese Academy of Sciences, Guangzhou 510640, People's Republic of China; University of Chinese Academy of Sciences, Beijing 100049, People's Republic of China;* orcid.org/0000-0001-5012-5192

Buqing Xu − *State Key Laboratory of Organic Geochemistry and Guangdong Key Laboratory of Environmental Protection and Resources Utilization, Guangzhou Institute of Geochemistry, Chinese Academy of Sciences, Guangzhou 510640, People's Republic of China*

Bolong Zhang − *State Key Laboratory of Organic Geochemistry and Guangdong Key Laboratory of Environmental Protection and Resources Utilization, Guangzhou Institute of Geochemistry, Chinese Academy of Sciences, Guangzhou 510640, People's Republic of China*

Sanyuan Zhu − *State Key Laboratory of Organic Geochemistry and Guangdong Key Laboratory of Environmental Protection and Resources Utilization, Guangzhou Institute of Geochemistry, Chinese Academy of Sciences, Guangzhou 510640, People's Republic of China*

Hairong Cheng − *School of Resource and Environmental Science, Wuhan University, Wuhan 430079, People's Republic of China*

Jun Li − *State Key Laboratory of Organic Geochemistry and Guangdong Key Laboratory of Environmental Protection and Resources Utilization, Guangzhou Institute of Geochemistry, Chinese Academy of Sciences, Guangzhou 510640, People's Republic of China;* orcid.org/0000-0002-3637-1642

Yingjun Chen − *Department of Environmental Science and Engineering, Fudan University, Shanghai 200438, People's Republic of China*

Complete contact information is available at: https://pubs.acs.org/10.1021/acs.est.0c00075

https://dx.doi.org/10.1021/acs.est.0c00075
Environ. Sci. Technol. 2020, 54, 5409−5418

Author Contributions

T.T. did the study, analyzed the data, and wrote the manuscript; Z.C. guided through the technical experiments, analyzed the data, and wrote the manuscript; G.Z. inspired and designed the study.

Notes

The authors declare no competing financial interest.

■ ACKNOWLEDGMENTS

This study was supported by the National Natural Science Foundation of China (41430645, 41703124, and 41773120), the National Key R&D Program of China (2017YFC0212000), the International Partnership Program of Chinese Academy of Sciences (132744KYSB20170002), Guangdong Foundation for Program of Science and Technology Research (2017B030314057), and the Natural Science Foundation of Guangdong Province of China (2018A050501009). We gratefully appreciate the people who contributed to the sample collection and all of the individuals and groups participating in this project. This is contribution No. IS-2850 from GIGCAS.

■ REFERENCES

(1) Toxicology and carcinogenesis studies of naphthalene (CAS no. 91-20-3) in F344/N rats (inhalation studies). *National Toxicology Program technical report series*; 2000 (500), pp 1−173.

(2) *Health effects support document for naphthalene. USEPA 822-R-03-005*; Office of Water, Health and Ecological Criteria Division: Washington, DC. 2003, 1−173.

(3) *ATSDR, Toxic profile for Naphthalene, 1-Methylnapthalene, and 2-Methylnapthalene*; U.S. Department of Health and Human Services, Agency for Toxic Substances and Disease Registry: Atlanta, GA, USA, 2005, 1−291.

(4) *IARC, Monographs on the evaluation of carcinogenic risks to humans*; International Agency for Research on Cancer (IARC),: Lyon, France, 2002; Vol. *82*, p 367.

(5) Chen, C. L.; Kacarab, M.; Tang, P.; Cocker, D. R., III SOA formation from naphthalene, 1-methylnaphthalene, and 2-methylnaphthalene photooxidation. *Atmos. Environ.* **2016**, *131*, 424−433.

(6) Chan, A. W. H.; Kautzman, K. E.; Chhabra, P. S.; Surratt, J. D.; Chan, M. N.; Crounse, J. D.; Kürten, A.; Wennberg, P. O.; Flagan, R. C.; Seinfeld, J. H. Secondary organic aerosol formation from photooxidation of naphthalene and alkylnaphthalenes: implications for oxidation of intermediate volatility organic compounds (IVOCs). *Atmos. Chem. Phys.* **2009**, *9* (9), 3049−3060.

(7) Kautzman, K. E.; Surratt, J. D.; Chan, M. N.; Chan, A. W. H.; Hersey, S. P.; Chhabra, P. S.; Dalleska, N. F.; Wennberg, P. O.; Flagan, R. C.; Seinfeld, J. H. Chemical composition of gas- and aerosol-phase products from the photooxidation of naphthalene. *J. Phys. Chem. A* **2010**, *114* (2), 913−934.

(8) Shakya, K. M.; Griffin, R. J. Secondary Organic Aerosol from Photooxidation of Polycyclic Aromatic Hydrocarbons. *Environ. Sci. Technol.* **2010**, *44* (21), 8134−8139.

(9) Kleindienst, T. E.; Jaoui, M.; Lewandowski, M.; Offenberg, J. H.; Docherty, K. S. The formation of SOA and chemical tracer compounds from the photooxidation of naphthalene and its methyl analogs in the presence and absence of nitrogen oxides. *Atmos. Chem. Phys.* **2012**, *12* (18), 8711−8726.

(10) Pye, H.; Seinfeld, J. A global perspective on aerosol from low-volatility organic compounds. *Atmos. Chem. Phys.* **2010**, *10*, 4377−4401.

(11) Huang, G.; Liu, Y.; Shao, M.; Li, Y.; Chen, Q.; Zheng, Y.; Wu, Z.; Liu, Y.; Wu, Y.; Hu, M.; Li, X.; Lu, S.; Wang, C.; Liu, J.; Zheng, M.; Zhu, T. Potentially important contribution of gas-phase oxidation of naphthalene and methylnaphthalene to secondary organic aerosol during haze events in beijing. *Environ. Sci. Technol.* **2019**, *53* (3), 1235−1244.

(12) Jia, C.; Batterman, S. A critical review of naphthalene sources and exposures relevant to indoor and outdoor air. *Int. J. Environ. Res. Public Health* **2010**, *7* (7), 2903−2939.

(13) Lu, R.; Wu, J.; Turco, R. P.; Winer, A. M.; Atkinson, R.; Arey, J.; Paulson, S. E.; Lurmann, F. W.; Miguel, A. H.; Eiguren-Fernandez, A. Naphthalene distributions and human exposure in Southern California. *Atmos. Environ.* **2005**, *39* (3), 489−507.

(14) Zhao, Y.; Nielsen, C. P.; Lei, Y.; McElroy, M. B.; Hao, J. Quantifying the uncertainties of a bottom-up emission inventory of anthropogenic atmospheric pollutants in China. *Atmos. Chem. Phys.* **2011**, *11* (5), 2295−2308.

(15) O'Malley, V. P.; Burke, R. A.; Schlotzhauer, W. S. Using GC−MS/Combustion/IRMS to determine the $^{13}C/^{12}C$ ratios of individual hydrocarbons produced from the combustion of biomass materials—application to biomass burning. *Org. Geochem.* **1997**, *27* (7−8), 567−581.

(16) Okuda, T.; Kumata, H.; Naraoka, H.; Takada, H. Origin of atmospheric polycyclic aromatic hydrocarbons (PAHs) in Chinese cities solved by compound-specific stable carbon isotopic analyses. *Org. Geochem.* **2002**, *33* (12), 1737−1745.

(17) Turner, N.; Jones, M.; Grice, K.; Dawson, D.; Ioppolo-Armanios, M.; Fisher, S. $\delta^{13}C$ of volatile organic compounds (VOCS) in airborne samples by thermal desorption-gas chromatography-isotope ratio-mass spectrometry (TD-GC-IR-MS). *Atmos. Environ.* **2006**, *40* (18), 3381−3388.

(18) Vitzthum von Eckstaedt, C.; Grice, K.; Ioppolo-Armanios, M.; Kelly, D.; Gibberd, M. Compound specific carbon and hydrogen stable isotope analyses of volatile organic compounds in various emissions of combustion processes. *Chemosphere* **2012**, *89* (11), 1407−1413.

(19) Sun, C.; Cooper, M.; Snape, C. E. Use of compound-specific $\delta^{13}C$ and δD stable isotope measurements as an aid in the source apportionment of polyaromatic hydrocarbons. *Rapid Commun. Mass Spectrom.* **2003**, *17* (23), 2611−2613.

(20) Bai, H.; Li, Y.; Peng, L.; Liu, X.; Liu, X.; Song, C.; Mu, L. Stable hydrogen isotope composition of n-alkanes in urban atmospheric aerosols in Taiyuan, China. *Atmos. Environ.* **2017**, *153*, 206−216.

(21) Vitzthum Von Eckstaedt, C.; Grice, K.; Ioppolo-Armanios, M.; Jones, M. $\delta^{13}C$ and δD of volatile organic compounds in an alumina industry stack emission. *Atmos. Environ.* **2011**, *45* (31), 5477−5483.

(22) von Eckstaedt, C. V.; Grice, K.; Ioppolo-Armanios, M.; Chidlow, G.; Jones, M. δD and $\delta^{13}C$ analyses of atmospheric volatile organic compounds by thermal desorption gas chromatography isotope ratio mass spectrometry. *Journal of Chromatography A* **2011**, *1218* (37), 6511−6517.

(23) Ya, M.; Xu, L.; Wu, Y.; Li, Y.; Zhao, S.; Wang, X. Fossil fuel-derived polycyclic aromatic hydrocarbons in the taiwan strait, China, and fluxes across the air-water interface. *Environ. Sci. Technol.* **2018**, *52* (13), 7307−7316.

(24) Andersson, A.; Deng, J.; Du, K.; Zheng, M.; Yan, C.; Skold, M.; Gustafsson, O. Regionally-varying combustion sources of the January 2013 severe haze events over eastern China. *Environ. Sci. Technol.* **2015**, *49* (4), 2038−2043.

(25) Bosch, C.; Andersson, A.; Krusa, M.; Bandh, C.; Hovorkova, I.; Klanova, J.; Knowles, T. D.; Pancost, R. D.; Evershed, R. P.; Gustafsson, Ö. Source apportionment of polycyclic aromatic hydrocarbons in central European soils with compound-specific triple isotopes ($\delta^{13}C$, $\Delta^{14}C$, and $\delta^{2}H$). *Environ. Sci. Technol.* **2015**, *49* (13), 7657−65.

(26) Jimenez, J. L.; Canagaratna, M. R.; Donahue, N. M.; Prevot, A. S. H.; Zhang, Q.; Kroll, J. H.; Decarlo, P. F.; Allan, J. D. Evolution of organic aerosols in the atmosphere. *Science* **2009**, *326* (5959), 1525−1529.

(27) Dobson, R.; Scheyer, A.; Rizet, A. L.; Mirabel, P.; Millet, M. Comparison of the efficiencies of different types of adsorbents at trapping currently used pesticides in the gaseous phase using the

https://dx.doi.org/10.1021/acs.est.0c00075
Environ. Sci. Technol. 2020, 54, 5409−5418

technique of high-volume sampling. *Anal. Bioanal. Chem.* **2006**, *386* (6), 1781−1789.
(28) Chuang, J. C.; Hannan, S. W.; Wilson, N. K. Field comparison of polyurethane foam and XAD-2 resin for air sampling for polynuclear aromatic hydrocarbons. *Environ. Sci. Technol.* **1987**, *21* (8), 798−804.
(29) Dreyer, A.; Weinberg, I.; Temme, C.; Ebinghaus, R. Polyfluorinated compounds in the atmosphere of the atlantic and southern oceans: evidence for a global distribution. *Environ. Sci. Technol.* **2009**, *43* (17), 6507−6514.
(30) Melymuk, L.; Bohlin, P.; Sáňka, O. e.; Pozo, K.; Klánová, J. Current Challenges in Air Sampling of Semivolatile Organic Contaminants: Sampling Artifacts and Their Influence on Data Comparability. *Environ. Sci. Technol.* **2014**, *48* (24), 14077−14091.
(31) Kim, M.; Kennicutt, M. C.; Qian, Y. Polycyclic Aromatic Hydrocarbon Purification Procedures for Compound Specific Isotope Analysis. *Environ. Sci. Technol.* **2005**, *39* (17), 6770−6776.
(32) Ziolkowski, L. A.; Druffel, E. R. Quantification of extraneous carbon during compound specific radiocarbon analysis of black carbon. *Anal. Chem.* **2009**, *81* (24), 10156.
(33) Moore, J. W.; Semmens, B. X. Incorporating uncertainty and prior information into stable isotope mixing models. *Ecology Letters* **2008**, *11* (5), 470−480.
(34) MixSIAR GUI user manual; http://github.com/brianstock/mixSIAR (accessed March 12, 2020).
(35) O'Malley, V. P.; Abrajano, T. A., Jr; Hellou, J. Determination of the $^{13}C/^{12}C$ ratios of individual PAH from environmental samples: Can PAH sources be apportioned? *Org. Geochem.* **1994**, *21* (6−7), 809−822.
(36) Batterman, S.; Chin, J. Y.; Jia, C.; Godwin, C.; Parker, E.; Robins, T.; Max, P.; Lewis, T. Sources, concentrations, and risks of naphthalene in indoor and outdoor air. *Indoor Air.* **2012**, *22* (4), 266−278.
(37) Eiguren-Fernandez, A.; Miguel, A. H.; Froines, J. R.; Thurairatnam, S.; Avol, E. L. Seasonal and spatial variation of polycyclic aromatic hydrocarbons in vapor-phase and PM 2.5 in Southern California urban and rural communities. *Aerosol Sci. Technol.* **2004**, *38* (5), 447−455.
(38) Zhang, Y.; Tao, S.; Shen, H.; Ma, J. Inhalation exposure to ambient polycyclic aromatic hydrocarbons and lung cancer risk of Chinese population. *Proc. Natl. Acad. Sci. U. S. A.* **2009**, *106* (50), 21063−21067.
(39) Schauer, J. J.; Kleeman, M. J.; Cass, G. R.; Simoneit, B. R. T. Measurement of emissions from air pollution sources. 4. C-1-C-27 organic compounds from cooking with seed oils. *Environ. Sci. Technol.* **2002**, *36* (4), 567−575.
(40) Liu, T.; Wang, Z.; Huang, D. D.; Wang, X.; Chan, C. K. Significant Production of Secondary Organic Aerosol from Emissions of Heated Cooking Oils. *Environ. Sci. Technol. Lett.* **2018**, *5* (1), 32−37.
(41) 157 villages in Huairou District complete coal to clean energy transformation (in chinese); https://www.sohu.com/a/279906494_161623; 2018 (accessed March 15, 2020).
(42) Ma, W. L.; Liu, L. Y.; Jia, H. L.; Yang, M.; Li, Y. F. PAHs in Chinese atmosphere Part I: Concentration, source and temperature dependence. *Atmos. Environ.* **2018**, *173*, 330−337.
(43) Liu, S.; Tao, S.; Liu, W.; Dou, H.; Liu, Y.; Zhao, J.; Little, M. G.; Tian, Z.; Wang, J.; Wang, L. Seasonal and spatial occurrence and distribution of atmospheric polycyclic aromatic hydrocarbons (PAHs) in rural and urban areas of the North Chinese Plain. *Environ. Pollut.* **2008**, *156* (3), 651−656.
(44) Chen, H.; Chen, W. Potential impact of shifting coal to gas and electricity for building sectors in 28 major northern cities of China. *Appl. Energy* **2019**, *236*, 1049−1061.
(45) Cheng, M.; Zhi, G.; Tang, W.; Liu, S.; Dang, H.; Guo, Z.; Du, J.; Du, X.; Zhang, W.; Zhang, Y. Air pollutant emission from the underestimated households' coal consumption source in China. *Sci. Total Environ.* **2017**, *580*, 641−650.
(46) Natural Resources Defense Council (NRDC). Report on scattered coal control in China 2017 (in Chinese); http://coalcap.nrdc.cn/pdfviewer/web/?15180772751437518672.pdf (accessed March 12, 2020).
(47) Air pollution targeted in 28 cities; http://en.cleanairchina.org/product/8931.html (accessed March 20, 2020).
(48) Sofuoglu, A.; Odabasi, M.; Tasdemir, Y.; Khalili, N. R.; Holsen, T. M. Temperature dependence of gas-phase polycyclic aromatic hydrocarbon and organochlorine pesticide concentrations in Chicago air. *Atmos. Environ.* **2001**, *35* (36), 6503−6510.
(49) Mao, S.; Li, J.; Cheng, Z.; Zhong, G.; Gan, Z. The contribution of biomass burning to ambient particulate polycyclic aromatic hydrocarbons at a regional background site in East China. *Environ. Sci. Technol. Lett.* **2018**, *5*, 56−61.
(50) Okuda, T.; Kumata, H.; Zakaria, M. P.; Naraoka, H.; Ishiwatari, R.; Takada, H. Source identification of Malaysian atmospheric polycyclic aromatic hydrocarbons nearby forest fires using molecular and isotopic compositions. *Atmos. Environ.* **2002**, *36* (4), 611−618.
(51) Glaser, B.; Dreyer, A.; Bock, M.; Fiedler, S.; Mehring, M.; Heitmann, T. Source apportionment of organic pollutants of a highway-traffic-influenced urban area in Bayreuth (Germany) using biomarker and stable carbon isotope signatures. *Environ. Sci. Technol.* **2005**, *39* (11), 3911−3917.
(52) Peng, L.; You, Y.; Bai, Z. P.; Zhu, T.; Xie, K. C.; Feng, Y. C.; Li, Z. Y. Stable carbon isotope evidence for origin of atmospheric polycyclic aromatic hydrocarbons in Zhengzhou and Urumchi, China. *Geochem. J.* **2006**, *40* (3), 219−226.
(53) Mcrae, C.; Snape, C. E.; Fallick, A. E. Variations in the stable isotope ratios of specific aromatic and aliphatic hydrocarbons from coal conversion processes. *Analyst* **1998**, *123* (7), 1519−1523.
(54) Sun, C.; Snape, C. E.; Mcrae, C.; Fallick, A. E. Resolving coal and petroleum-derived polycyclic aromatic hydrocarbons (PAHs) in some contaminated land samples using compound-specific stable carbon isotope ratio measurements in conjunction with molecular fingerprints. *Fuel* **2003**, *82* (15), 2017−2023.
(55) Sheesley, R. J.; Krus, M.; Krecl, P.; Johansson, C.; Gustafsson, Ö. Source apportionment of elevated wintertime PAHs by compound-specific radiocarbon analysis. *Atmos. Chem. Phys.* **2009**, *9* (10), 3347−3356.
(56) Mandalakis, M.; Gustafsson, Ö.; Alsberg, T.; Egeback, A.-L.; Reddy, C. M.; Xu, L.; Klanova, J.; Holoubek, I.; Stephanou, E. G. Contribution of biomass burning to atmospheric polycyclic aromatic hydrocarbons at three European background sites. *Environ. Sci. Technol.* **2005**, *39* (9), 2976−2982.
(57) Mandalakis, M.; Gustafsson, O.; Reddy, C. M.; Xu, L. Radiocarbon apportionment of fossil versus biofuel combustion sources of polycyclic aromatic hydrocarbons in the Stockholm metropolitan area. *Environ. Sci. Technol.* **2004**, *38* (20), 5344−5349.
(58) Beckman, J.; Gooch, E.; Gopinath, M.; Landes, M. Market impacts of China and India meeting biofuel targets using traditional feedstocks. *Biomass Bioenergy* **2018**, *108*, 258−264.
(59) Krauss, M.; Wilcke, W.; Martius, C.; Bandeira, A. G.; Garcia, M. V. B.; Amelung, W. Atmospheric versus biological sources of polycyclic aromatic hydrocarbons (PAHs) in a tropical rain forest environment. *Environ. Pollut.* **2005**, *135* (1), 143−154.
(60) Musa Bandowe, B. A.; Ruckamp, D.; Braganca, M. A.L.; Laabs, V.; Amelung, W.; Martius, C.; Wilcke, W. Naphthalene production by microorganisms associated with termites: Evidence from a microcosm experiment. *Soil Biol. Biochem.* **2009**, *41* (3), 630−639.
(61) Xu, L.; Zheng, M.; Ding, X.; Edgerton, E. S.; Reddy, C. M. Modern and Fossil Contributions to Polycyclic Aromatic Hydrocarbons in PM2.5 from North Birmingham, Alabama in the Southeastern U.S. *Environ. Sci. Technol.* **2012**, *46* (3), 1422.
(62) Yuan, B.; Liu, Y.; Shao, M.; Lu, S.; Streets, D. G. Biomass burning contributions to ambient VOCs species at a receptor site in the Pearl River Delta (PRD), China. *Environ. Sci. Technol.* **2010**, *44* (12), 4577−4582.

https://dx.doi.org/10.1021/acs.est.0c00075
Environ. Sci. Technol. 2020, 54, 5409−5418

(63) Mastral, A. M.; Callén, M. S. A Review on Polycyclic Aromatic Hydrocarbon (PAH) Emissions from Energy Generation. *Environ. Sci. Technol.* **2000**, *34* (15), 3051−3057.
(64) Xu, S.; Liu, W.; Tao, S. Emission of Polycyclic Aromatic Hydrocarbons in China. *Environ. Sci. Technol.* **2006**, *40* (3), 702−8.
(65) McRae, C.; Love, G. D.; Murray, I. P.; Snape, C. E.; Fallick, A. E. Potential of gas chromatography isotope ratio mass spectrometry to source polycyclic aromatic hydrocarbon emissions. *Anal. Commun.* **1996**, *33*, 331−333.
(66) Mcrae, C.; Sun, C. G.; Snape, C. E.; Fallick, A. E.; Taylor, D. $\delta^{13}C$ values of coal-derived PAHs from different processes and their application to source apportionment. *Org. Geochem.* **1999**, *30*, 881−889.
(67) Bergmann, F. D.; Laban, N. M. F. H. A.; Meyer, A. H.; Martin, E.; Meckenstock, R. U. Dual (C, H) isotope fractionation in anaerobic low molecular weight (poly)aromatic hydrocarbon (PAH) degradation: potential for field studies and mechanistic implications. *Environ. Sci. Technol.* **2011**, *45* (16), 6947−6953.

https://dx.doi.org/10.1021/acs.est.0c00075
Environ. Sci. Technol. 2020, 54, 5409−5418